Advanced Industrial and Engineering Polymer Research xxx (xxxx) xxx

Contents lists available at ScienceDirect

Advanced Industrial and Engineering Polymer Research

journal homepage: http://www.keaipublishing.com/aiepr

Surface grafting POSS to improve the hydrophobicity and fire safety of polyrotaxane based smart phase change materials

Guang-Zhong Yin [a, *], Mei-Hui Zhou [b], María Fernanda Acosta [a], Pedro Rincón Arévalo [a]

[a] Escuela Politécnica Superior, Universidad Francisco de Vitoria, Ctra. Pozuelo-Majadahonda Km 1,800, 28223, Pozuelo de Alarcón, Madrid, Spain
[b] Materials Science and Engineering Area, Escuela Superior de Ciencias Experimentales y Tecnología, Universidad Rey Juan Carlos, Calle Tulipán S/n, 28933 Móstoles, Madrid, Spain

ARTICLE INFO

Article history:
Received 11 October 2022
Received in revised form
23 December 2022
Accepted 29 December 2022

Keywords:
Phase change materials
Polyrotaxane
POSS
Fire safety
Shape memory polymer

ABSTRACT

Polyethylene Glycol (PEG)-based flexible phase change materials have broad and practical application value in thermal management of flexible electronic devices. Considering the typical application cases and safety of phase change materials (PCMs), in this work, we grafted molecular nanoparticles, POSS, with both hydrophobic and flame retardant functions to the surface of PLR sheets through amidation reaction. The successful grafting of POSS has been fully verified by Fourier-transform infrared spectroscopy, energy dispersive spectroscopy and surface contact angle. The formation of the cross-linked structure and the introduction of POSS make the phase change latent heat of the phase change material slightly decrease from 102.4 J g^{-1} to 94.4 J g^{-1}, but there is still a high retention rate. It is worth pointing out that the PCMs have excellent shape stability and leakage resistance, cycle stability, and shape memory performance (R_f-99%, R_r-99%). The introduce of cross-linked structure and POSS significantly enhanced the Young's modulus and tensile strength of the PCM. The surface POSS functionalization endowed the PCM with significantly enhanced hydrophobicity. Specifically, the contact angle of the material was significantly increased from 71° for PLR to 123° for POSS-PLR, and it also had enhanced fire safety with pHRR reduction by 18.4% and THR reduction by 19.1%.

1. Introduction

Nowadays, the demand for energy and the consumption of fossil fuels continues to grow, especially in countries with rapid economic development. Furthermore, the environmental and human health consequences of greenhouse gases and pollutants released by the transportation industry are significant, necessitating the development of new and renewable energy sources [1,2]. Designing new energy storage materials and efficient utilization is imperative for promoting sustainable development and alleviating environmental pollution [3]. Thermal energy is one of the main energy types employed in domestic industrial applications, constituting up to 70% of global energy consumption [4]. Phase change materials (PCMs) store/release isothermal energy during the phase change process and show a high heat storage capacity. They can be employed in various applications such as thermal energy storage, thermal management of electronics [5], regulation of building temperature, while simultaneously increase the thermal comfort for humans [6,7], and battery thermal management systems [8]. Organic PCMs including paraffin wax, fatty acids, fatty alcohols, and glycols are pertinent in the "high technology" area [9]. Among of them, flexible PCM is a key property to utilize PCMs for thermal management of advanced electronic devices, the human body, and many other applications. Therefore, it is highly desired to develop PCMs that possess the flexibility to be explored for widespread applications [10,11].

In the previous work, it is reported the Polyrotaxane (PLR) based smart PCM [12], PLR based high performance PCM with high latent heat and adjustable phase transition temperature [13]. The researchers further introduced the water-soluble flame retardant to improve the fire safety of the PCMs [14,15].

PLR-based PCMs are water soluble [16]. Like most PEG-based PCMs, PLR-based PCMs are difficult to use in wet conditions, or moisture tends to make them ineffective. Thermal management components, both in construction and in electronics, require a certain degree of moisture/water resistance. For conquering the risk of accidental humidification and water leakage, to further ensure the normal operation of electronic devices, moisture

* Corresponding author.
E-mail address: amos.guangzhong@ufv.es (G.-Z. Yin).

https://doi.org/10.1016/j.aiepr.2022.12.006

Please cite this article as: G.-Z. Yin, M.-H. Zhou, M.F. Acosta *et al.*, Surface grafting POSS to improve the hydrophobicity and fire safety of polyrotaxane based smart phase change materials, Advanced Industrial and Engineering Polymer Research, https://doi.org/10.1016/j.aiepr.2022.12.006

absorption resistance is very important in electronic applications. We intend to modify the surface of PLR based PCM sheet to enhance its moisture resistance. Compared with the homogeneous introduction of modifiers, surface modification saves the modifier contents, and can also maximize the retention of the properties of the PCM bulk and maintain a higher proportion of latent heat of phase transition. This also facilitates the first shaping of the material to obtain the desired sample size and shape.

Polyhedral oligomeric silsesquioxanes (POSS), a class of hybrid molecules with an inorganic silicon oxygen cage, which can generally improve thermal stability and mechanical properties [17]. As a typical hydrophobic modifier [18–20], POSS is also an excellent flame retardant modifier [21–23]. Considering the necessity of moisture resistance in practical application of PCM, as well as the hydrophobicity and flame retardancy of POSS itself, in this work, we intend to modify the surface of PCM by chemical means by coating POSS. The successful introduction of POSS is expected to improve the mechanical properties, moisture resistance and combustion safety of the material to a certain extent.

2. Experimental

2.1. Materials and methods

Polyethylene oxide (PEO) with a weight average molar mass of 9×10^5 g mol^{-1}, α-Cyclodextrin (α-CD, ≥99.8%), Hexamethylene Diisocyanate (HDI, ≥99.0% (GC)), Tin(II) 2-ethylhexanoate, and *n*-Hexane were both purchased from Sigma Aldrich and used as received. Deionized water is made in our laboratory. AminopropylIsobutyl POSS (POSS—NH_2) was purchased from Hybrid and without further treatment.

Synthesis of polyrotaxane (PLR). Polyrotaxane was synthesized according to the report elsewhere [24] Typically, PEO (3 g) was dissolved in H_2O (80 mL) at 80 °C, and then α-CD with 20% mass ratio was slowly added. After stirring for overnight at room temperature, the reaction mixture was cooled down and kept at 4 °C for 72 h to yield the corresponding inclusion complex solutions.

Preparation of PEO PLR films. The aqueous ***PLR*** was casted directly into 10 × 10 cm^2 Polytetrafluoroethylene mold. After evaporation at room temperature for 72 h, the flexible films were obtained with thickness at about 0.1 mm. The films then further dried in vacuum oven at 50 °C for additional 24 h.

Crosslinking and POSS surface coating. HDI (10 mL) was mixed in *n*-hexane (90 mL) with 2 drops of Tin (II) 2-ethylhexanoate. The PLR thin sheet was immersed into the solution at 60 °C overnight. The sheet was washed 3 times by pure *n*-hexane (after drying in vacuum oven at 45 °C for additional 24 h, *c*-PLR was obtained) and immersed into saturated POSS solution (in *n*-hexane) directly. The reaction system was kept at 60 °C overnight. The POSS coated PLR sheet was washed 3 times by pure *n*-hexane and dried in vacuum oven at 45 °C for 24 h, giving rise to POSS-PLR sample.

X-ray diffraction (XRD) patterns of the films were obtained in reflection mode using a X'PERT-PRO diffractometer with Cu Kα (λ = 0.1542 nm) and Ni filter.

Attenuated Total Reflection-Fourier Transform Infrared (ATR–FTIR) spectra of the films were recorded from 500 cm^{-1} to 4000 cm^{-1} with a 4 cm^{-1} resolution (32 scans) using corresponding instruments (Jasco FT/IR-6100) at room temperature.

Energy dispersive spectroscopy (EDS) were carried out on the apparatus (SEM, EVO MA15, Zeiss) and FIB-FEG SEM dual-beam microscope (FIBFESEM) (Helios NanoLab 600i, FEI). Prior to the observation, the conductive gold layer was sprayed.

Differential scanning calorimetry (DSC) analysis was performed for each film (5–10 mg) using a TA-Q200 in a N_2 atmosphere (50 mL min^{-1}). The crystallinity (φ_c%) were calculated in the second heating run from −40 °C to 100 °C at heating rate of 10 °C min^{-1} by the equation [17]:

$$\varphi_c\% = \frac{\Delta H_m}{\omega_i \Delta H_m^0} \times 100\% \quad (1)$$

where, ΔH_m (J g^{-1}) represented the measured enthalpies of melting, ΔH_m^0 (J g^{-1}) was the melting enthalpy for a 100% crystalline material and ω_i (%) was the fraction of the component *i* in the sample. The value taken for ΔH_m^0 of PEO was 196.4 J g^{-1} [25]

Cycle stability test. Sample POSS-PLR was selected for 80 cycles. Both heating and cooling procedures were used to test at 10 °C min^{-1} to calculate the change of exothermic and endothermic heat as well as the enthalpy efficiency and phase change temperatures.

Thermogravimetric analysis (TGA) of the films was performed using a TGA in both N_2 and air atmosphere from 25 °C to 700 °C at 10 °C min^{-1} using a TA-Q50 instrument. All the samples are tested when it is freshly fabricated.

Form stability. The sample was cut into a disc of 13.50 ± 0.05 mm with a cutter. The samples were heated at different temperatures (30 °C and 80 °C) to detect the form stability (leakage or shape change).

Tensile test. The tensile test samples were dumbbell-shaped with dimensions of 75 mm × 5 mm × 0.1 mm, complying with ISO 527-2 (1996) standard. An Instron 5966 (USA), universal tensile testing machine was utilized to carry out the tensile tests with a 2000-N load cell and an initial length of 30 mm at a rate of 50 mm • min^{-1} test speed. Minimum 3 specimens were tested for each sample to obtain a reliable average value and standard deviations.

Shape Memory performance. For shape programming and recovery, each sample (obtained by hot press) was cut from a film with dimensions 30 mm (length) × 2.5 mm (width) × 0.1 mm (thickness). During testing, the sample was firstly stretched above the melting temperature from a preloaded length to a length of 250%. The shape fixity ratio, R_f, and the shape recovery ratio, R_r, were used to quantify the shape memory behavior. R_f was related to the fixation of the temporary shape and was a measure of the fix ability of a mechanical deformation. R_r described to what extent the original shape can be recovered. The percentage of shape fixing, R_f(N), and shape recovery, R_r (N), were calculated using the following equations [20]:

$$R_f(N) = \frac{l_f(N) - l_i(N-1)}{l_p(N) - l_i(N-1)} \times 100\% \quad (2)$$

$$R_r(N) = \frac{l_p(N) - l_r(N)}{l_p(N) - l_i(N-1)} \times 100\% \quad (3)$$

where l_p was the length before releasing the applied load, l_f was the length obtained after releasing the applied load, l_i was the initial sample length, l_r was the final length after heating with no applied load, and N is the cycle number (3 cycles were included in the tests: C1, C2 and C3. The concrete process are as follow: (1) the sample (with length of l_i) was deformed at 80 °C with strain 250% (l_p), (2) the sample was cooled to room temperature under constant tensile stress to freeze the extended strain (l_p). Subsequently, the applied stress was released, and the strain remains constant due to the restrain of crystalline domains (l_f); (3) the sample was heated up to 80 °C again, and the extended strain started to recover when the temperature exceeded T_m of the sample (l_r).

Contact angle. The water contact angle (WCA) measurement was carried out by applying 2 μ L of the water droplet onto the porous PLLA sample surface under ambient laboratory conditions at room temperature.

Micro combustion calorimeter (MCC). MCC was executed in the facility (MCC-1, FTT) based on the oxygen-depletion mechanism. The combustion heat with consuming 1 g oxygen was fixed at 13.1 kJ with 4% derivation. The oxygen depletion was recorded via flow meter and O_2 meter. 5–10 mg sample was heated from 150 °C to 750 °C at 1 K s^{-1} under nitrogen. The anaerobic thermal-degradation products were mixed with oxygen stream prior to conveying to 900 °C combustion furnace. Heat release rate (HRR, W g^{-1}) and total heat release (THR, kJ g^{-1}) were generated by unit-weight sample.

3. Results and discussion

3.1. Synthesis and structure characterization of PLR and PLR-POSS

The synthesis of PLR is reported in the previous study (Fig. 1a) [12] In order to ensure sufficient hydroxyl groups (active sites) for POSS reaction, and high latent heat of phase transition, PLR-20 was designed and synthesized in this work, and then PLR sheet with a thickness of 0.1 mm were obtained by solvent casting (Fig. 1b). After cross-linking by HDI (20 wt % in *n*-hexane) (Fig. 1c) POSS coating and drying (Fig. 1d) we obtained POSS coated PLR based phase change materials (POSS-PLR). We first characterized the successful progress of the crosslinking reaction by gel content, as shown in Fig. 1e. PLR is fully water soluble. The gel contents of *c*-PLR and POSS-PLR were calculated to be 25.35% and 27.84%, respectively. This indicates that the cross-linking reaction between HDI and α-CD occurred. Furthermore, we verified by FTIR that the surface was enriched with active −NCO groups (2265.6 cm^{-1}), as shown in Fig. 1f and illustrated in Fig. 1c. The signal at 1624.1 cm^{-1} is the amide I band, and 1571.3 cm^{-1} is the amide II band [17] When the POSS was fully grafted, the −NCO signal disappeared completely, indicating that the surface −NCO were fully reacted with POSS, and POSS was successfully introduced onto the surface of the PCM sample, accordingly. In addition, the Si−O−Si signal at 1095.4 cm^{-1} which is derived from POSS cubic cage and the urea bond at 1687.9 cm^{-1} appeared, further indicating that the amino group on

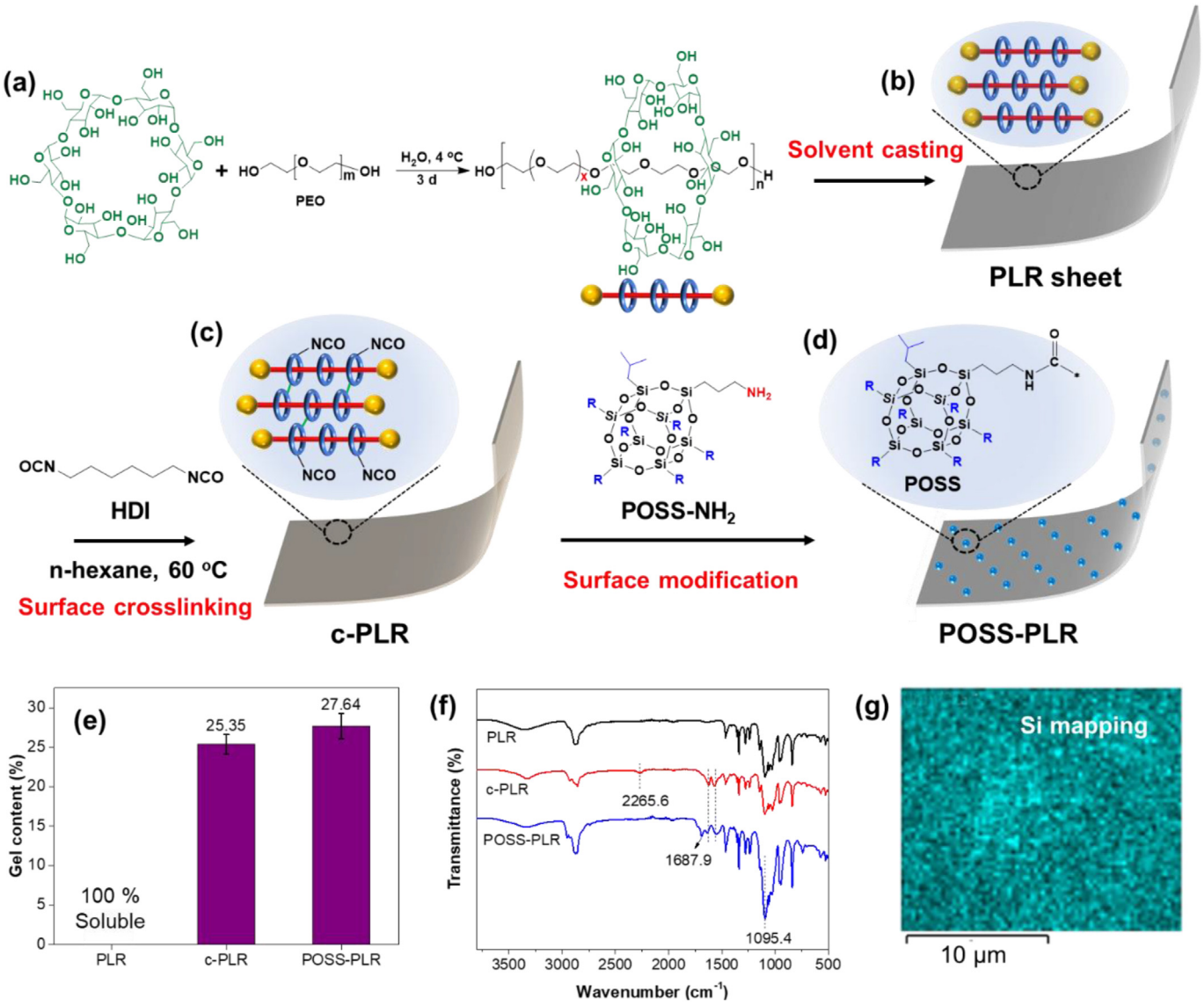

Fig. 1. (a) PLR synthesis route, (b) PLR sheet illustration, (c) *c*-PLR with surface −NCO groups, (d) POSS-PLR sheet illustration, (e) Gel content results of the 3 samples, (f) FTIR spectra of all the 3 PLRs, and (g) Si mapping of POSS-PLR surface.

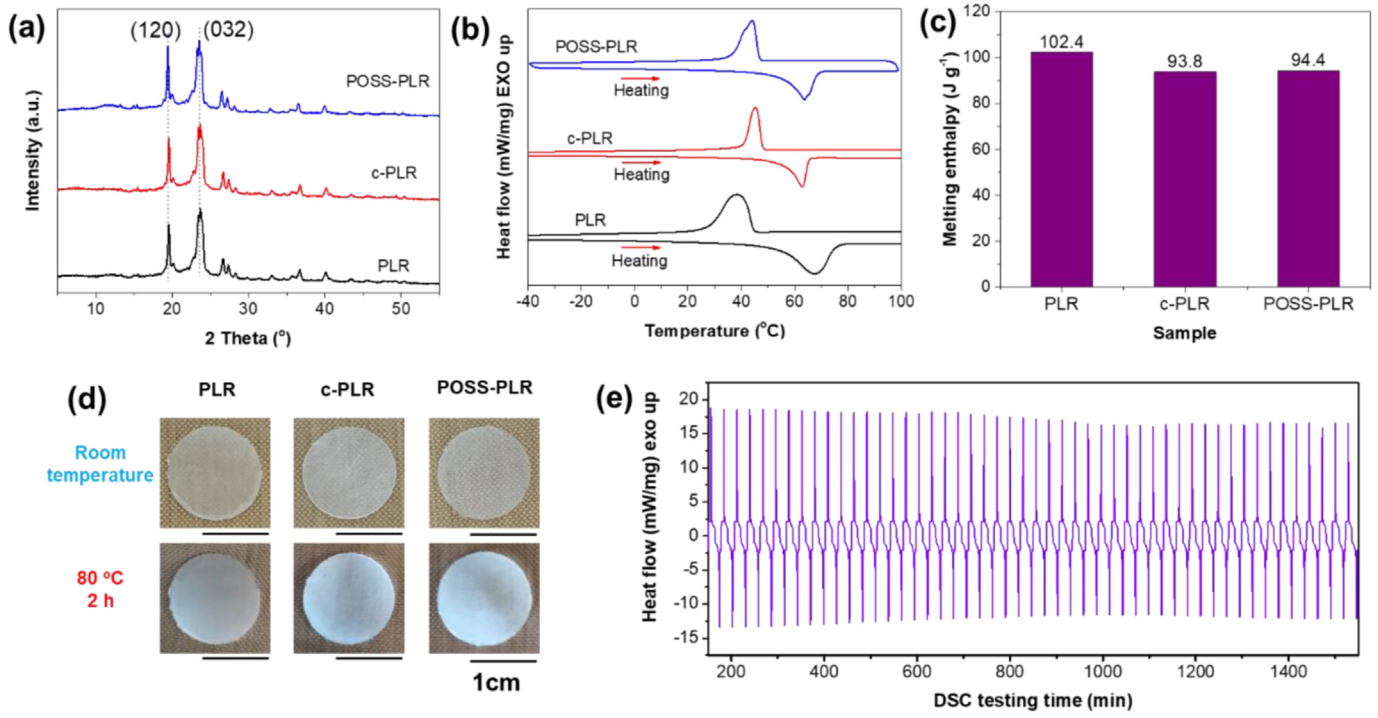

Fig. 2. (a) XRD curves of sample PLR, *c*-PLR and POSS-PLR; (b) Nonisothermal DSC curves of all the a samples; (c) melting enthalpies of PCMs at heating rate of 10 °C min^{-1}; (d) form stability of the samples at different temperatures: (top), room temperature, (bottom) 80 °C for 2 h; and (e) DSC cycle curves of PCMs (sample POSS-PLR).

Table 1
DSC data list of the PLRs.

Samples	$T_{m,\ peak}$ (°C)	T_s (°C)	H_m (J g^{-1})	H_s (J g^{-1})	Heat lose (%)	Crystallinity (%)
PLR	67.48	38.33	102.40	98.81	3.51	62.57
c-PLR	62.85	45.24	93.81	93.06	0.80	57.32
POSS-PLR	63.75	44.01	94.42	94.22	0.21	57.69

Note: the data were collected based on the curves with heating or cooling rata at 10 °C min^{-1}.

POSS reacted with −NCO on the surface of *c*-PLR. Another direct proof was the uniform EDs Si mapping in Fig. 1g also fully illustrates the successful introduction of POSS. Based on the gel content results and equations (1)–(3), we can estimate that the grafting amount of POSS in POSS-PLR is about 3.1 wt%.

$$\frac{M_{crosslinking}}{M_{crosslinking}+M_{soluble}} = Gel\ content_{c-PLR} \quad (4)$$

$$\frac{M_{crosslinking}+M_{POSS}}{M_{crosslinking}+M_{soluble}+M_{POSS}} = Gel\ content_{POSS-PLR} \quad (5)$$

Therefore,

$$POSS\,\% = \frac{M_{POSS}}{M_{crosslinking}+M_{soluble}+M_{POSS}} \times 100\% \quad (6)$$

where, M_{POSS}, $M_{crosslinking}$, and $M_{soluble}$ are the mass of coated POSS, gel part and the uncross-linked parts of the corresponding sample.

3.2. Phase change and shape memory properties

Fig. 2a shows the XRD curves of PLR, *c*-PLR and POSS-PLR. The two strong peaks at 2 theta of 19° and 23° for PEO film are attributed to the (120) and (032) planes, respectively of PEO crystals [26] Fig. 2b shows the nonisothermal melting peaks of PLR-20% determined at different heating rates. Combined with no difference in XRD signals and little change in crystallinity detected by DSC (as listed in Table 1), it can be seen that cross-linking and the introduce of POSS have no significant effect on the crystallization of PLR. This is also the reason why the latent heat of phase transition does not change too much. As shown in Fig. 2c, the latent heat of phase transition has no difference from the combined XRD signal of PLR and little change in crystallinity detected by DSC (as listed in Table 1). Typically, the latent heat slightly decreased from the 102.4 J g^{-1} to 93.8 J g^{-1} and 94.4 J g^{-1} for *c*-PLR and POSS-PLR, respectively.

The percentage of heat lose (η, %) was evaluated by equation (7):

$$\eta = \frac{\Delta H_m - \Delta H_s}{\Delta H_m} \times 100\ \% \quad (7)$$

where, ΔH_m (J g^{-1}) was the latent heat value of the PCMs, and ΔH_s (J g^{-1}) is solidification enthalpy.

The heat lose and ΔH_m were also listed in Table 1. As shown in Table 1, the PCMs exhibited a relatively high-phase change enthalpy (94.4 J g^{-1}) (Fig. 2c). The percentage of heat loss for POSS-PLR between endothermic and exothermic cycles was quite low (<3.51%),

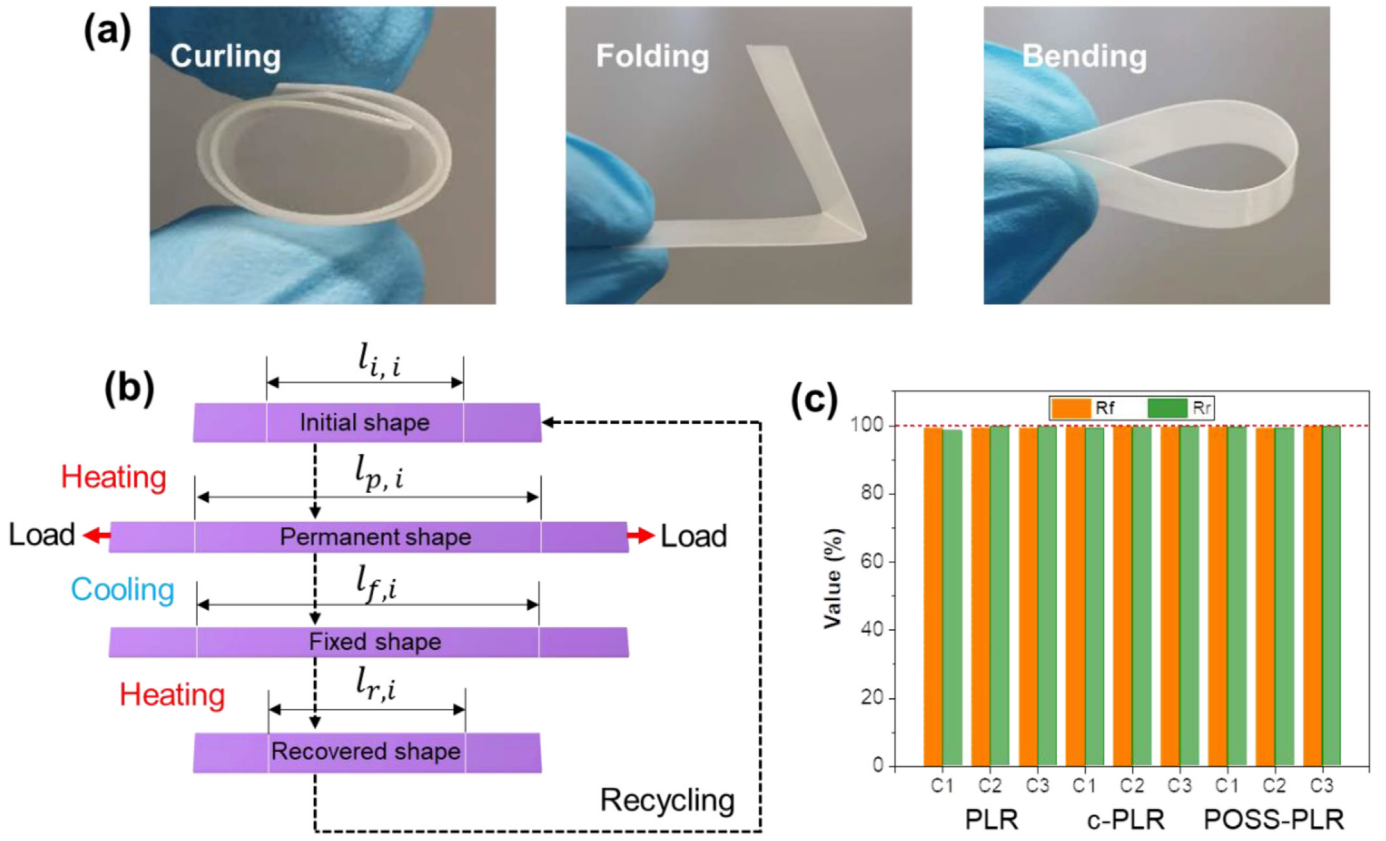

Fig. 3. (a) The sheet images to show its flexibility: the sample can be curled, folded and bent; (b) schematic diagram of shape memory test procedure, and (c) the R_f and R_r testing results (3 cycles (C1, C2 and C3) for each sample.

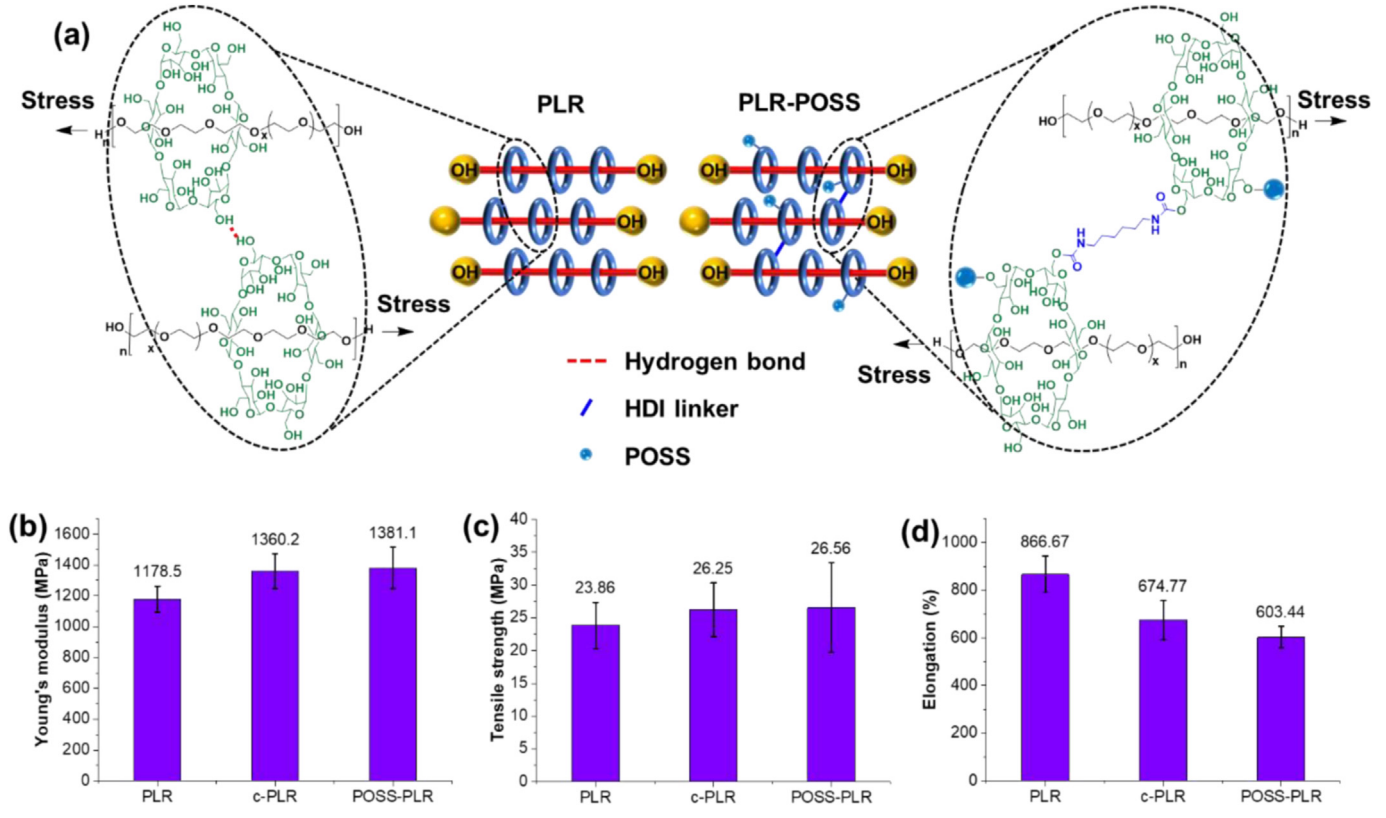

Fig. 4. (a) The illustration for the mechanical enhancement mechanism, (b) Young's modules, (c) Tensile strength, and (d) elongation at break.

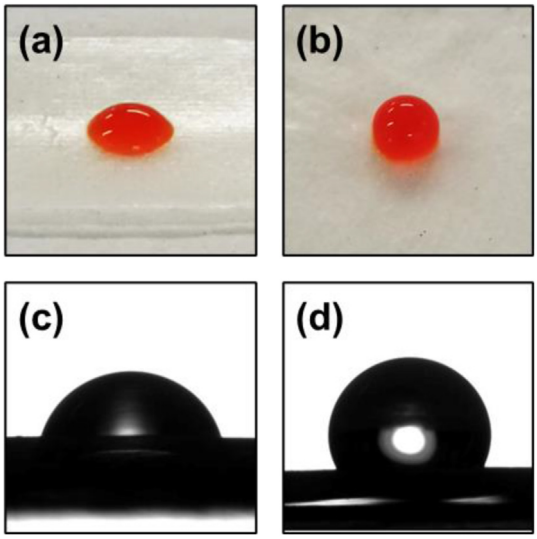

Fig. 5. (a) Water droplet with Methyl Orange on PLR surface, (b) Water droplet with Methyl Orange on POSS-PLR surface, (c) Contact angle results of sample PLR (WCA = (71 ± 2)°), and (d) Contact angle results of sample POSS-PLR (WCA = (123 ± 3)°).

which indicated the crosslink and POSS introduce will not induce the heat loss of PEO in PCMs.

The photos of pure PEO and PLRs using hot plate treatment at different temperature are shown in Fig. 2d. All the PLRs showed no significant changes in appearance. In addition, no leakage was observed during the entire heating process even when the temperature reached 80 °C, which was much higher than the phase-transition temperature of PLR ($T_{m,\ peak}$ = 67.5 °C). These results indicate that the PLRs have excellent form stabilities. This is mainly because when PLR is crosslinked, the micro crystallization or micro aggregation of α-CD plays a role in the physical crosslinking point, so that the shape of the sample can be greatly maintained.

The PCMs films had clear melting and crystallization temperatures in the heating and cooling processes, respectively, and had good cycle performance (Fig. 2e) after 80 cycles. The PLR films are therefore regarded as high-performance form-stable phase change materials for thermal energy storage. As shown in Fig. 3a, it is clearly depicted that the samples can be curled, folded and bent, which indicates the POSS-PLR has ultra-high flexibility.

The examination of heat-induced shape memory properties focused on a uniaxial force of stretching to a specified percent elongation using the procedure as shown in Fig. 3b. Fig. 3c showed the values for strain fixity (R_f) and strain recovery (R_r) for each sample within 3 cycles, namely, C1, C2 and C3. As it can be seen, the

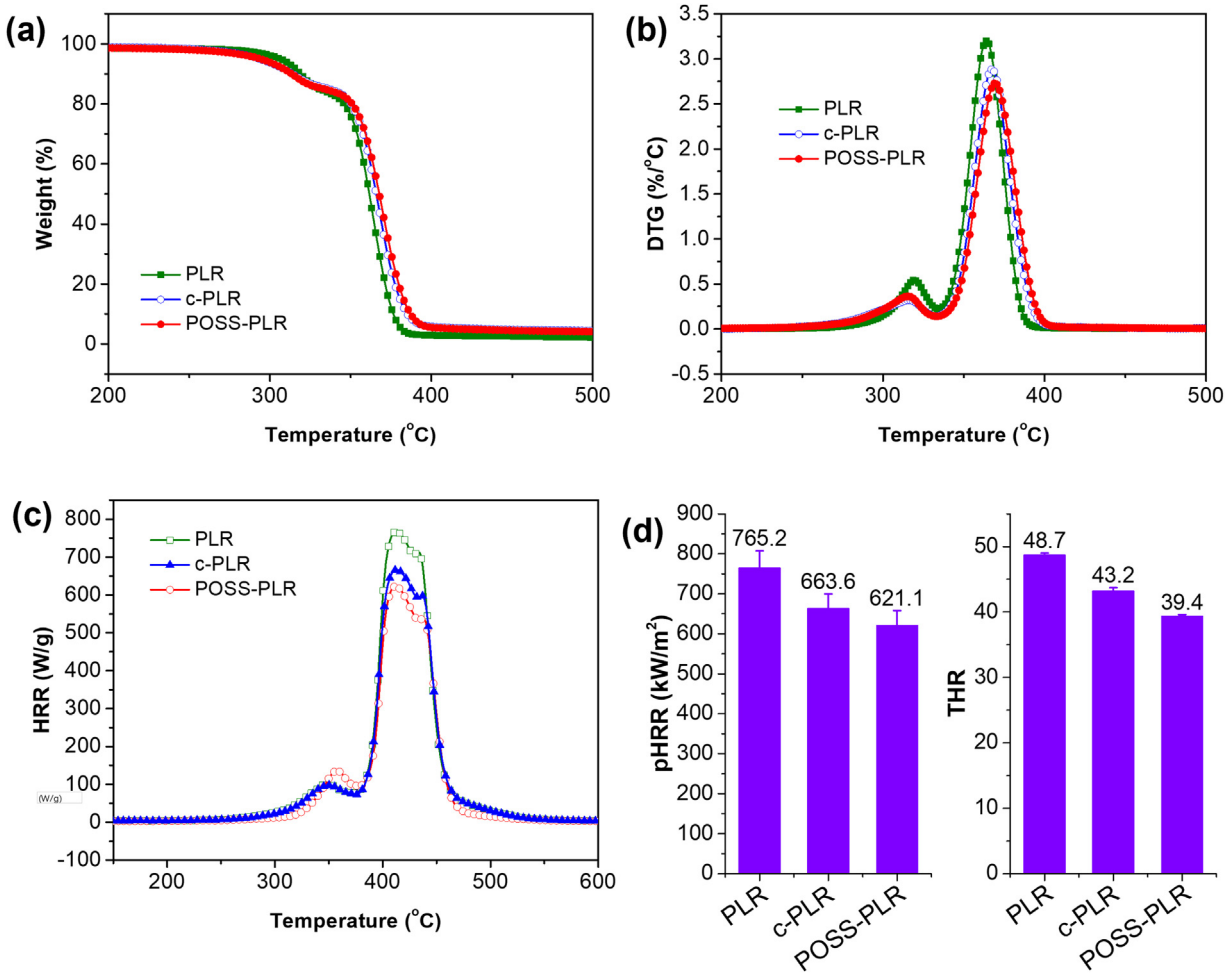

Fig. 6. (a) TGA curves obtained in N_2 atmosphere, (b) DTG curves (in N_2) of samples PLR, *c*-PLR and POSS-PLR; (c) MCC curves, and (d) pHRR and THR values of samples PLR, *c*-PLR and POSS-PLR.

Table 2
TGA results and MCC parameters.

Samples	$T_{max,1}$ (°C)	$T_{max,2}$ (°C)	Char residue at 600 °C (%)	pHRR (kW m^{-2})	THR(MJ m^{-2})
PLR	319.3	364.0	1.8	765.2	48.7
c-PCR	316.2	367.6	3.9	663.6	43.2
POSS-PLR	315.5	369.4	3.7	621.1	39.4

R_f is with ~99% of the initial strain after unloading of the stress, and the R_r is with ~99% of the strain recovering instantaneously. Notably, its ultra-high flexibility, remolding ability and excellent shape memory properties provide a convenient way for the intelligent heat treatment packaging of electronic devices or some other items.

3.3. Mechanical properties

In PLR, α-CD forms crystallites that act as physical cross-linking points [27], Therefore, PLR also has higher tensile strength and Young's modulus. When POSS is introduced, the cyclodextrins will be cross-linked through chemical bonds to enhance the interaction between PLRs. It has the effect of enhancing modulus and strength (Fig. 4a). Specifically, as shown in Fig. 4b, the Young's modulus of PLR (obtained by solvent casting) was about 1178.5 MPa, which increased significantly to 1360.2 MPa after HDI cross-linking. The significant increase in modulus may be due to the rivet effect of cyclodextrin in the PLR as shown in Fig. 3a, and cyclodextrin is the physical steric hindrance that contributes to the resistance to deformation. In the cross-linking system, the cyclodextrin is linked by the HDI reaction, and its resistance to deformation is significantly improved. The tensile strength of PLR increased from 23.86 MPa to 26.25 MPa (Fig. 4c). With the introduction of POSS surface, both Young's modulus and tensile strength were slightly improved on the basis of *c*-PLR. After the material is modified by cross-linking and POSS coating, the elongation at break decreases while the modulus and strength are enhanced (Fig. 4d).

3.4. Hydrophobicity, thermal stability and fire safety

Fig. 5a–d proved the hydrophobicity enhancement by the surface POSS functionalization. Typically, as shown in Fig. 5a and b, the water droplet stands with different status on the PLR and POSS-PLR surface. The water contact angles (WCA) of sample PLR (WCA = 71°), was significantly increased to sample POSS-PLR with value of 123°.

Thermogravimetric analysis (TGA) and derivative TGA (DTG) analyses were carried out to determine the thermal stability of the PCMs. The corresponding results are presented in Fig. 6a and b, and Table 2. As it can be seen, all the PCMs underwent a two-step degradation process. The first step involved the degradation of the α-CD at ~320 °C. The second step occurred at approximately above 350 °C, which corresponds to the decomposition of the PEO chain. As it is reported, the decomposition starts earlier, following a different pathway with more incomplete decomposition and a higher residue [28] The behavior of an earlier start of decomposition and a higher residue is often found for samples with good fire-safe performance. This was similar to the ordinary phosphorous containing modifiers which could reduce the degradation temperature of the PCMs and changed the decomposition history [29,30] After modification, char of the material increases slightly (from 1.8% of PLR to 3.7% of POSS-PLR).

MCC was further used to characterize the heat release performance of the materials. Fig. 6c presents the MCC curve of all samples. It can be seen that all the samples also have two maximum heat release peaks at ~350 °C (decomposition of α-CD) and 410 °C (decomposition of PEO). It is found that the peak value of PLR is gradually shifted earlier compared with PLR, which is consistent with the results observed in TGA curves (Fig. 6a and b). Most importantly, the pHRR of PLRs decreased with the introduce of POSS. For POSS-PLR, the pHRR was decreased by 18.8%, and THR decreased by 19.1% than that of PLR. The change trend of THR can be seen intuitively in Fig. 6d. The specific data are listed in Table 3. It is clear from the results that the fire safety of the modified material is improved to a certain extent due to the decrease of pHRR and THR.

Table 3
Tensile parameters.

Samples	Young's modules (MPa)	Elongation at break(%)	Tensile strength (MPa)
PLR	1178.5 ± 184.9	866.7 ± 76.5	23.9 ± 3.5
c-PCR	1360.2 ± 114.2	674.8 ± 82.4	26.2 ± 4.1
POSS-PLR	1381.1 ± 136.0	603.4 ± 45.9	26.6 ± 6.9

4. Conclusions

PLR with POSS coating was successfully synthesized. Compared with the pristine PLR, the thermal stability in the air and tensile properties of PLR were improved to a certain extent. Typically, the Young's modulus and tensile strength of the PLR film are 1178.5 MPa and 23.9 MPa, and remarkably increased to 1381.1 MPa and 26.6 MPa, respectively. The PCMs possess outstanding shape-fixing and recovery properties (both shape-fixing and recovery ratios are about 99%). Further with the relatively high phase transition enthalpy (94.4 J g^{-1}), excellent cycle performance, the PLR films are therefore promising sustainable and advanced form stable phase change materials for energy storage. Notably, with the introduction of surface POSS, the hydrophobicity of the material was significantly improved, and its contact angle was significantly improved from 71° to 123°. In addition, fire safety has also been improved to a certain extent, with pHRR decreasing by 18.8% and THR decreasing by 19.1%.

Declaration of competing interest

The authors declare that they have no known competing financial interests or personal relationships that could have appeared to influence the work reported in this paper.

References

[1] J. Luo, D. Zou, Y. Wang, S. Wang, L. Huang, Chem. Eng. J. 430 (2022), 132741.
[2] A. Mitra, R. Kumar, D.K. Singh, Z. Said, J. Energy Storage 53 (2022), 105195.
[3] D.G. Atinafu, B.Y. Yun, S. Yang, H. Yuk, S. Wi, S. Kim, Energy Storage Mater. 42 (2021) 164–184.
[4] K. Yuan, J. Shi, W. Aftab, M. Qin, A. Usman, F. Zhou, Y. Lv, S. Gao, R. Zou, Adv. Funct. Mater. 30 (2020), 1904228.
[5] Y.-J. Lan, S.-J. Chang, C.-C. Li, J. Mater. Chem. 5 (2017) 25583–25593.
[6] M. Gonçalves, R.M. Novais, L. Senff, J. Carvalheiras, J.A. Labrincha, Build. Environ. 205 (2021), 108281.
[7] C. Cheng, F. Gong, Y. Fu, J. Liu, J. Qiao, J. Mater. Res. Technol. 15 (2021) 1970–1983.
[8] W. Wu, J. Liu, M. Liu, Z. Rao, H. Deng, Q. Wang, X. Qi, S. Wang, Energy Convers. Manag. 221 (2020), 113145.
[9] D.C. Hyun, N.S. Levinson, U. Jeong, Y. Xia, Angew. Chem. Int. Ed. 53 (2014) 3780–3795.
[10] Q. Huang, X. Li, G. Zhang, Y. Kan, C. Li, J. Deng, C. Wang, Appl. Energy 309 (2022), 118434.
[11] J. Shi, M. Qin, W. Aftab, R. Zou, Energy Storage Mater. 41 (2021) 321–342.
[12] G.-Z. Yin, J. Hobson, Y. Duan, D.-Y. Wang, Energy Storage Mater. 40 (2021) 347–357.
[13] G.-Z. Yin, A. Marta López, X.-M. Yang, X. Ao, J. Hobson, D.-Y. Wang, Chem. Eng. J. 444 (2022), 136421.

[14] G.-Z. Yin, A. Marta López, X.-M. Yang, W. Ye, B. Xu, J. Hobson, D.-Y. Wang, Eur. Polym. J. 173 (2022), 111262.
[15] G.-Z. Yin, X.-M. Yang, J.L.D. Palencia, J. Hobson, A.M. López, D.-Y. Wang, J. Energy Storage 56 (2022), 105853.
[16] G.-Z. Yin, X.-M. Yang, A.M. López, M.-T. Wang, W. Ye, B. Xu, D.-Y. Wang, Int. J. Biol. Macromol. 222 (2022) 429–437.
[17] G. Yin, D. Zhao, X. Wang, Y. Ren, L. Zhang, X. Wu, S. Nie, Q. Li, RSC Adv. 5 (2015) 79070–79080.
[18] M. Li, Y. Fang, C. Liu, M. Zhou, X. Miao, Y. Pei, Y. Yan, W. Xiao, H. Qiu, L. Wu, Front. Chem. Sci. Eng. 16 (2022) 1247–1258.
[19] Z. Lingru, C. Zhaoyu, H. Ling, J. Juan, M. Tao, L. Junyan, Prog. Org. Coating 170 (2022), 106972.
[20] G. Yin, L. Zhang, Q. Li, J. Polym. Res. 23 (2016) 138.
[21] Y. Feng, W. Wu, Z. Wang, T. Zhao, Polym. Adv. Technol. 33 (2022) 1190–1201.
[22] V.-H. Nguyen, C. Manh Vu, H.V. Thi, Compos. Interfac. 28 (2021) 843–858.
[23] W. Wu, W. Zhao, X. Gong, Q. Sun, X. Cao, Y. Su, B. Yu, R.K.Y. Li, R.A.L. Vellaisamy, J. Mater. Sci. Technol. 101 (2022) 107–117.
[24] S. Choi, T.-w. Kwon, A. Coskun, J.W. Choi, Science 357 (2017) 279–283.
[25] K. Chrissopoulou, K.S. Andrikopoulos, S. Fotiadou, S. Bollas, C. Karageorgaki, D. Christofilos, G.A. Voyiatzis, S.H. Anastasiadis, Macromolecules 44 (2011) 9710–9722.
[26] G.-Z. Yin, X.-M. Yang, J. Hobson, A.M. López, D.-Y. Wang, Compos. Commun. 30 (2022), 101057.
[27] S. Uenuma, R. Maeda, H. Yokoyama, K. Ito, Macromolecules 52 (2019) 3881–3887.
[28] R.S. Kappes, T. Urbainczyk, U. Artz, T. Textor, J.S. Gutmann, Polym. Degrad. Stabil. 129 (2016) 168–179.
[29] S. Hao, W. Zhu, H. Huang, M. Yang, J. Zhang, ChemistrySelect 4 (2019) 13952–13958.
[30] P. Zhu, S. Sui, B. Wang, K. Sun, G. Sun, J. Anal. Appl. Pyrol. 71 (2004) 645–655.